

We are IntechOpen, the world's leading publisher of Open Access books Built by scientists, for scientists

6,900

Open access books available

186,000

International authors and editors

200M

Downloads

Our authors are among the

154

Countries delivered to

TOP 1%

most cited scientists

12.2%

Contributors from top 500 universities



WEB OF SCIENCE™

Selection of our books indexed in the Book Citation Index
in Web of Science™ Core Collection (BKCI)

Interested in publishing with us?
Contact book.department@intechopen.com

Numbers displayed above are based on latest data collected.
For more information visit www.intechopen.com



Ductile Mode Micro Laser Assisted Machining of Silicon Carbide (SiC)

Deepak Ravindra, Saurabh Virkar and John Patten
Western Michigan University
USA

1. Introduction

This chapter is divided into three parts: (1) background research, (2) experimental work and (3) simulations on ductile mode micro laser assisted machining. The origin and science behind ductile regime machining will briefly be discussed prior to discussing the experimental and simulated study conducted on SiC. Although the results of both studies (experimental and simulation) are not intended for direct comparison, the main objective of both studies are similar, that is to analyze the effects of laser heating/thermal softening on ductile mode machining of single crystal 4H-SiC.

1.1 Background

Although silicon carbide (SiC) has been around since 1891, it was not until the mid 1990's that this material was introduced into the precision manufacturing industry. SiC is well known for its excellent material properties, high durability, high wear resistance, light weight and extreme hardness. However, SiC is also well known for its low fracture toughness, extreme brittleness and poor machinability. SiC is one of the advanced engineered ceramics designed to operate in extreme environments. This material is pursued as both a coating and structural material due to its unique properties, such as:

- Larger energy bandgap and breakdown field allowing it to be used in high-temperature, high-power and radiation-hard environments
- Mechanical stiffness, expressed by its high Young's modulus (Gao et al., 2003)
- Desirable tribological properties, such as wear resistance and self-lubricating (Ashurst et al., 2004)

SiC is commercially available in various forms/phases (polytypes) such as single crystal, polycrystalline (sintered and CVD) and amorphous. The most common polytypes of SiC are 2H, 3C, 4H, 6H, and 15R. The numbers refer to the number of layers in the unit cell and the letter designates the crystal structure, where C=cubic, H=hexagonal, and R=rhombohedral. In this study, only one polytype will be discussed: 4H. The 4H polytype is a single crystal.

1.2 Ductile Regime Machining

Materials that are hard and brittle, such as semiconductors, ceramics and glasses, are amongst the most challenging to machine. When attempting to machine ceramics, such as SiC, especially to improve the surface finish, it is important to carry out a 'damage free' machining operation. This often can be achieved by ductile mode machining (DMM) or in other words machining a nominally hard and brittle material in the ductile regime. Material removal processes can be considered in terms of fracture dominated mechanisms or localized plastic deformation. A fracture dominant mechanism for ceramics, i.e., brittle fracture, can result in poor surface finish (surface damage) and also compromises on material properties and performance (Ravindra et al., 2007).

The insight into the origins of the ductile regime during single point diamond turning (SPDT) of semiconductors and ceramics was provided by the research done by Morris, et al in 1995 in collaboration with one of the current authors (Patten). A detailed study of machining chips (debris) and the resultant surface was studied (analyzed using a TEM) to evaluate evidence of plastic material deformation. This seminal research concluded that the machining chips were plastically formed and are amorphous (not due to oxidation) due to the back transformation of a pressure induced phase transformation, and the machining debris (chips) contain small amounts of micro-crystalline (brittle) fragments.

According to the grinding research carried out by Bifano et al. in 1991, there are two types of material removal mechanisms associated with the machining process: ductile; plastic flow of material in the form of severely sheared machining chips, and brittle; material removal through crack propagation. This previous research discusses several physical parameters that influence the ductile to brittle transition in grinding of brittle materials. The researchers were successful in performing ductile mode grinding on brittle materials. However, these researchers did not propose or confirm a model or suitable explanation for the origin of this ductile regime. Bifano et al. also proposed a model defining the ductile to brittle transition of a nominally brittle material based on the material's brittle fracture properties and characteristics. A critical depth of cut model was introduced based on the Griffith fracture propagation criteria. The critical depth of cut (d_c) formula is as follows:

$$d_c = (E \cdot R) / H^2 \quad (1)$$

where E is the elastic modulus, H is the hardness and R is the fracture energy. The value of the fracture energy (R) can be evaluated using the relation:

$$R \sim K_c^2 / H \quad (2)$$

where K_c is the fracture toughness of the material. The above two equations can be combined to represent the critical depth (d_c) as a measure of the brittle transition depth of cut:

$$d_c \sim (E / H) \cdot (K_c / H)^2 \quad (3)$$

The researchers were successful in determining a correlation between the calculated critical depth of cut and the measured depth (grinding infeed rate). The constant of proportionality

was estimated as to be 0.15 and this is now added into Equation (2.3) to generate a more accurate empirical equation:

$$d_c \sim 0.15 \cdot (E / H) \cdot (K_c / H)^2 \quad (4)$$

1.3 Chip Formation

A critical depth, d_c is determined before any ductile mode machining operation is carried out. Any depth beyond or exceeding the critical depth, which is also known as the Ductile to Brittle Transition (DBT) depth, will result in a brittle cut. Since the equipment used in the current study (Universal Micro-Tribometer by CETR) is a load controlled (and not a depth controlled) machine, thrust force calculations were carried out for corresponding required depths of cuts. The Blake and Scattergood ductile regime machining model (as shown in Fig. 1) was used to predict the required thrust force for a desired depth of cut (Blake & Scattergood, 1991). In this model it is assumed that the undesirable fracture damage (which extends below the final cut surface) will originate at the critical chip thickness (t_c), and will propagate to a depth, y_c . This assumption is consistent with the energy balance theory between the strain energy and surface energy (Bifano et al., 1991).

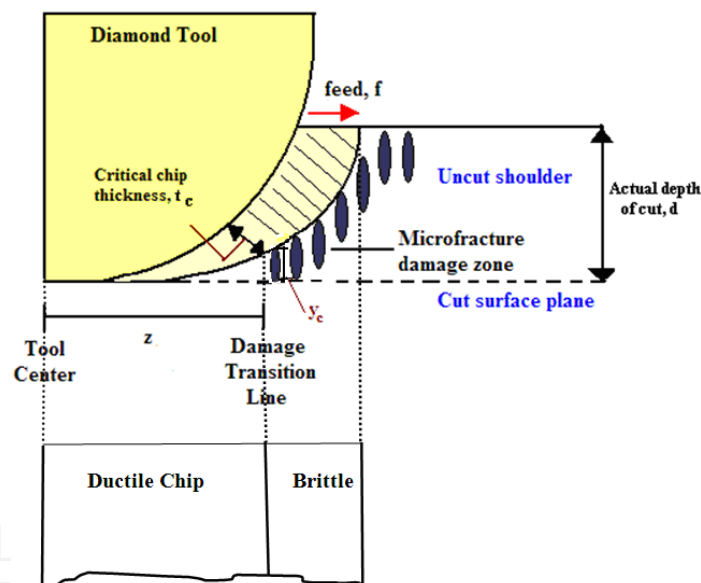


Fig. 1. Model for ductile regime machining

In general, the ductile-to-brittle transition (DBT) is a function of variables such as tool geometry (rake and clearance angle, nose and cutting edge radius), feed rate, and depth of cut.

1.4 High Pressure Phase Transformation (HPPT)

Although SiC is naturally very brittle, micro/nanomachining this material is possible if sufficient compressive stress is generated to cause a ductile mode behavior, in which the material is removed by plastic deformation instead of brittle fracture. This micro-scale phenomenon is also related to the High Pressure Phase Transformation (HPPT) or direct amorphization of the material (Patten et al., 2005). Fig. 2 shows a graphical representation of the highly stressed (hydrostatic and shear) zone that results in ductile regime machining.

Patten and Gao state that ceramics in general undergo a phase transformation to an amorphous phase after a machining process. This transformation is a result of the High Pressure Phase Transformation (HPPT) that occurs when the high pressure and shear caused by the tool (during the chip generation process) is suddenly released after a machining process. This phase transformation is usually characterized by the amorphous remnant that is present on the workpiece surface and within the chip. This amorphous remnant is a result of a back transformation from the high pressure phase to the atmospheric pressure phase due to the rapid release of pressure in the wake of the tool. There are two types of material removal mechanisms during machining: ductile mechanism and the brittle mechanism (Bifano et al., 1991). In the ductile mechanism, plastic flow of material in the form of severely sheared machining chips occur, while material removal is achieved by the intersection and propagation of cracks in the brittle fracture mechanism. Due to the presence of these two competing mechanisms, it is important to know the DBT depths (or critical size) associated with these materials before attempting a machining operation.

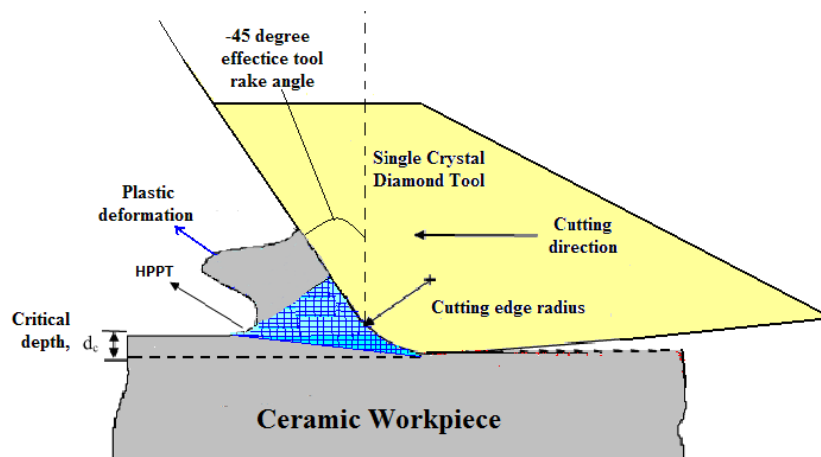


Fig. 2. A ductile machining model of brittle materials

Fig. 2 shows a ductile cutting model showing the high compressive stress and plastically deformed material behavior in brittle materials. A -45° rake angle tool is demonstrated in the above schematic as a negative rake angle tool yields in higher compressive stresses at the tool-workpiece interface.

1.5 Challenges in Ductile Regime machining of Ceramics

Since the hardness of SiC is approximately 30% of the hardness of diamond, machining SiC with a diamond tool is an extremely abrasive process. As a result of the abrasive material removal process, there are several limitations in terms of machining parameters that have to be considered. The primary limitation in the process of ductile mode machining is to not exceed the critical depth of cut or the DBT depth of the material. Exceeding the DBT depth during the machining process will result in fracture and thus leaving a poor surface finish. Another important parameter during machining is the feed. In general, lower feed rates result in a better surface finish however; lower feed rates also result in more tool wear due to the longer track length covered by the tool during machining. Tool wear can be crucial when trying to improve the surface finish of a SiC workpiece. Any wear along the cutting

edge radius (rake and flank wear) will directly affect the machined surface finish, possibly causing cracks and fracture. A small chipped area or crack in the tool tip could potentially grow during the machining process, eventually causing the tool to fail. Tool failure at times can be observed in the cutting forces during the machining process. In general, low cutting forces are desired to minimize the diamond tool wear. The micro laser assisted machining (μ -LAM) process, which will be discussed in the next few sections, shows positive results in addressing the challenges faced in conventional ductile regime machining of SiC.

2. Experimental Study on Ductile Mode μ -LAM

2.1 Introduction to μ -LAM

Semiconductors and ceramics share common characteristics of being nominally hard and brittle, which stems from their covalent chemical bonding and crystal structure. These materials are important in many engineering applications, but are particularly difficult to machine in traditional manufacturing processes due to their extreme hardness and brittleness. Ceramics have many desirable properties, such as excellent wear resistance, chemical stability, and high strength even at elevated temperatures. All of these properties make them ideal candidates for tribological, semiconductor, MEMS and optoelectronic applications. In spite of all these characteristics, the difficulty during machining and material removal has been a major obstacle that limited the wider application of these materials (Jahanmir et al., 1992). The plastic deformation of these nominally brittle materials at room temperature is much less than in metals, which means they are more susceptible to fracture during material removal processes. Surface cracks generated during machining are subsequently removed in lapping and polishing processes, which significantly increases the machining time and cost. Machining mirror-like surface finishes contribute significantly to the total cost of a part. In some cases, grinding alone can account for 60-90% of the final product cost (Wobker & Tonshoff, 1993). In this context, developing a cost effective method to achieve a flawless surface in ultra fine surface machining of an optical lens or mirror has become a challenge. In many engineering applications, products require a high quality surface finish and close tolerances to function properly. This is often the case for products made of semiconductor or ceramic materials. The real challenge is to produce an ultra precision surface finish in these nominally brittle materials at low machining cost.

Current limitations for brittle material machining include the high cost of processing and low product reliability. The cost is mainly due to the high tool cost, rapid tool wear, long machining time, low production rate and the manufacturing of satisfactory surface figure and form. The low product reliability is primarily due to the occurrence of surface/subsurface damage, i.e., cracks, and brittle fracture. In order to develop a suitable process, ductile regime machining, considered to be one of the satisfactory precision machining techniques, has been continuously studied over the last two decades (Blake & Scattergood, 1990; Blackley & Scattergood, 1994; Morris et al., 1995; Leung et al., 1998; Sreejith & Ngoi, 2001; Yan et al., 2002; Patten et al., 2003; Patten et al., 2005). Laser assisted micro/nano machining is another important development in this direction (Dong & Patten, 2007; Rebro et al., 2002).

In past research, it has been demonstrated that ductile regime machining of these materials is possible due to the high pressure phase transformation (HPPT) occurring in the material

caused by the high compressive and shear stresses induced by the single point diamond tool tip (Ravindra et al., 2009; Ravindra & Patten, 2008). To further augment the ductile response of these materials, traditional scratch/single point diamond turning tests are coupled with a micro-laser assisted machining (μ -LAM) technique (Shayan et al., 2009). A schematic of the basic underlining concept of the μ -LAM process is shown in Fig. 3. This hybrid method could potentially increase the critical depth of cut (DoC) (larger DBT depth) in ductile regime machining, resulting in a higher material removal rate. μ -LAM was previously successfully carried out on single crystal Si yielding a greater DBT (for the scratch performed with laser heating)(Ravindra et al., 2010).

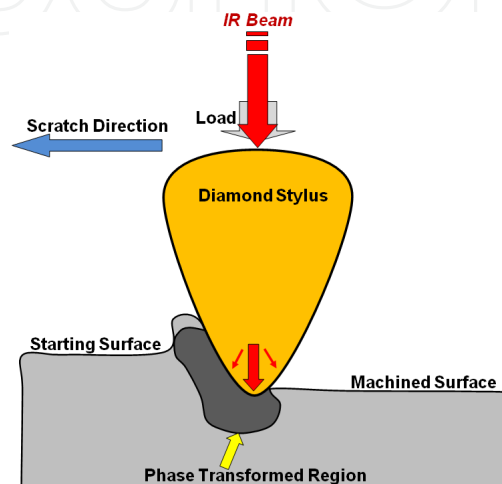


Fig. 3. A schematic cross-section of the μ -LAM process

The objective of the current study is to determine the effect of laser heating (using the μ -LAM process) on the material removal of single crystal 4H-Silicon Carbide (SiC) using scratch testing. The scratch tests were carried out to examine the effect of temperature in thermal softening of the high pressure phases formed under the diamond tip. There were two studies done from these scratch experiments: studying the laser heating effect on the DBT of the material and evaluating the thermal softening and relative hardness as a result of irradiation of the laser beam at a constant cutting speed. The effects of laser heating were studied by verifying the depths of cuts and the nature of the scratches (i.e. ductile, DBT or brittle) for diamond stylus scratch tests carried out on single crystal SiC with increasing loads (thrust force). The load range was selected such that the scratches show both ductile and brittle response (with a DBT region within the scratch). Cutting forces and three-dimensional cutting surface profiles (using a white light interferometer) were investigated.

2.2 Experimental Process

The scratch tests were performed on a Universal Micro-Tribometer (UMT) which is produced by the Center for Tribology Research Inc. (CETR). This equipment was developed to perform comprehensive micro-mechanical tests of coatings and materials at the micro scale. This system facilitates cutting speeds as low as $1\mu\text{m}/\text{sec}$ at nanometric cutting depths. The tribometer is a load controlled device where the required thrust force (F_z) is applied by the user to obtain the desired DoC (based on the tool geometry and workpiece material properties). The unit is equipped with a dual-axis load cell that is capable of constantly

monitoring the thrust and cutting forces (F_x); obtained as an output parameter from the cutting experiment. A typical scratch test setup along with the μ -LAM system is shown in Fig. 4. All scratch tests were performed on a single crystal 4H-SiC wafer. All cuts were performed on the $\{1010\}$ plane along the $\langle 1010 \rangle$ direction.

A 90° conical single crystal diamond stylus (with a spherical end tip radius of $5\mu\text{m}$) was used as the scratch tool. The details of the diamond tip attachment were depicted in Fig. 5. An infrared (IR) diode fiber laser ($\lambda=1480\text{nm}$ and $P_{\text{max}}=400\text{mW}$,) with a Gaussian profile with a beam diameter of $\sim 10\mu\text{m}$ was used in this study. The laser beam is guided through a $10\mu\text{m}$ fiber optic cable to the ferrule, which is attached to the diamond stylus. The μ -LAM system is configured in such a way that the laser beam passes through the diamond tip and impinges on the work piece material at the tool work piece interface (contact) (Dong, 2006).

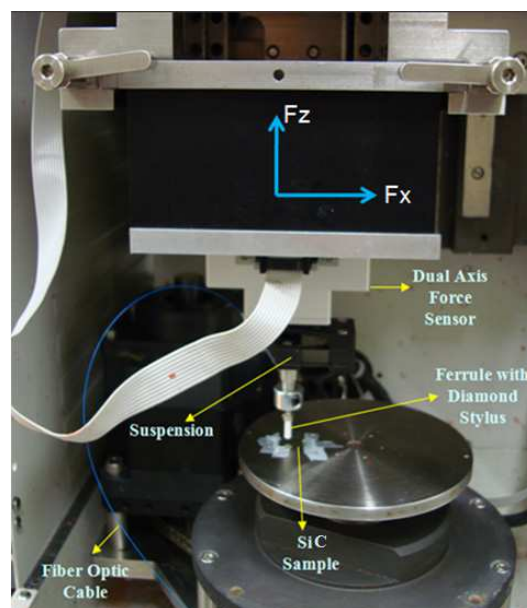


Fig. 4. μ -LAM setup on the Universal Micro Tribometer

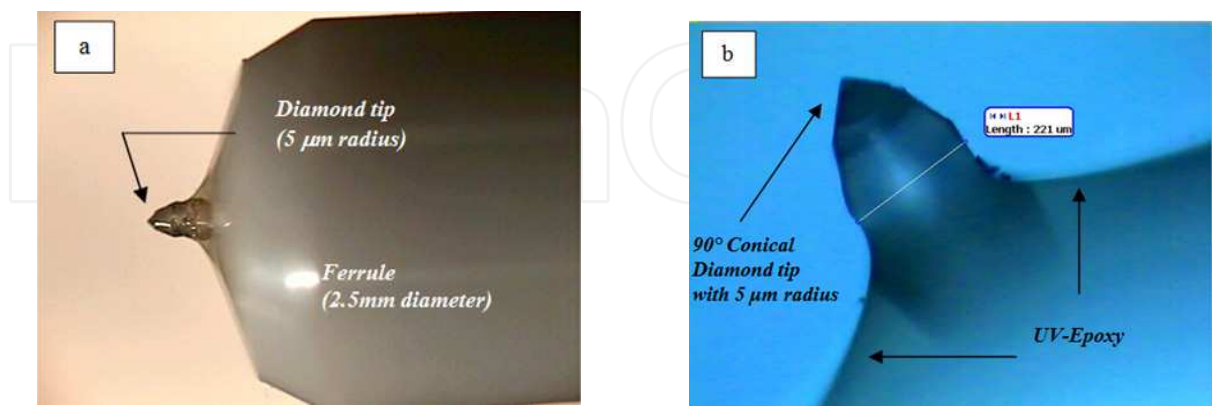


Fig. 5. Diamond tip attachment: (a) $5\mu\text{m}$ radius diamond tip attached on the end of the ferrule using epoxy, (b) Close up on diamond tip embedded in the solidified epoxy

Scratch tests were chosen to be the principal method of investigation in this study as it is a better candidate for evaluating machining conditions than indenting because the mechanics during scratching are more applicable to the machining process such as single point diamond turning (SPDT). In this study, two conditions of scratches were performed: with and without laser heating. The scratches were carried out at low cutting speeds ($1 \mu\text{m}/\text{sec}$) in order to maximize the thermal softening of the material during the laser heating. Scratch lengths of $500 \mu\text{m}$ were produced on the SiC wafer specimen. The loads were increased linearly with time from 2 mN to 70 mN along the scratch. The scratch test parameters are summarized in Table 1.

Scratch Number	Load Range, F_z (mN)	Machining Condition	Cutting Speed, (μm)	Laser Power (mW)
1	2 - 70 mN	No Laser	1	0
2	2 - 70 mN	With Laser	1	350

Table 1. Scratch testing parameters

**350mW is the laser power, approximately 150mW is actually delivered to the work piece material, the balance of the laser power is lost due to scattering and reflections.*

2.3 Experimental Results & Discussion

Fig. 6 shows two scratches that represent the two conditions: without (scratch 1) and with laser heating (scratch 2). The load range (2-70 mN) performed on these scratches was ideal for this study as it had both the ductile and brittle regime along the same scratch. The DBT is identified somewhere between the ductile and brittle regime of the scratch using optical microscopy, white light interferometry and force analysis (from variations in cutting forces). It is seen in Fig. 6 that the scratch performed without laser heating exhibits brittle fracture along the cut before, i.e., at a shallower depth, than the scratch performed with laser heating.

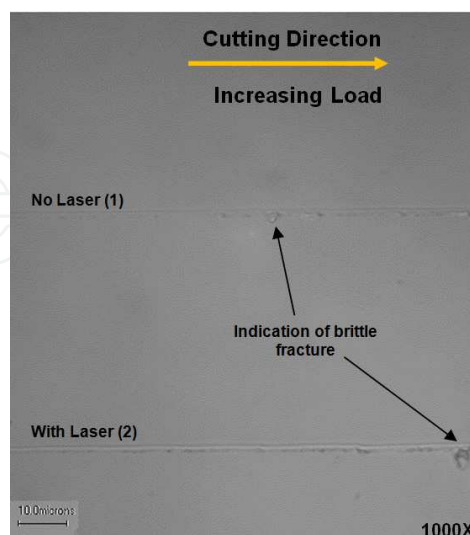


Fig. 6. Micrograph showing brittle fracture along the scratch

In this study, there were two different analyses done based on the results obtained from the scratch tests. The first analysis compares the depth and cutting forces (F_x) for a constant thrust force (F_z) for both cutting conditions (with and without laser heating) to see the effect of thermal softening on the material. For this analysis, scratches analyzed for both conditions were in the ductile regime. The results summarized in Table 2 show that for the same amount of applied thrust force ($F_z = 30\text{mN}$), the scratch performed with laser heating yielded a greater depth of cut (145nm vs. 95nm). It is also evident that cutting forces were equal for both these conditions for an equal applied thrust force (although the scratch performed with laser heating was significantly deeper). A scratch without laser heating done at higher loads to result in a depth of 145nm will most definitely result in higher cutting forces due to the hardness of the material (Shayan et al., 2009).

The second analysis done was to study the effects of laser heating on the DBT of the material. To determine this, two-dimensional scratch/groove profiles obtained using a white light interferometric profilometer were analyzed. Fig. 7 shows the cross-section of the two scratches taken at an equal thrust force of approximately 35mN. It can be seen that the scratch performed with laser heating (left) exhibits a perfectly ductile behavior whereas the scratch done without laser heating (right) indicates slight fracture (brittle behavior) of the material. The DBT depth identified for the scratch performed without laser heating just before the point of fracture is approximately 105nm. The brittle behavior is identified by the imperfect pattern of the groove edge which is a representation of the stylus imprint on the material. It is important to note from Fig. 7, that the scratch performed without laser heating is (apparently) deeper (210nm vs. 113nm) as it is difficult to control the depth when the material removal mechanism is brittle (i.e. difficult to predict the depth due to fracture of the material). The clear and defined edges that depict the stylus imprint is a good indication of ductile response of the material (as seen in the scratch performed with laser heating).

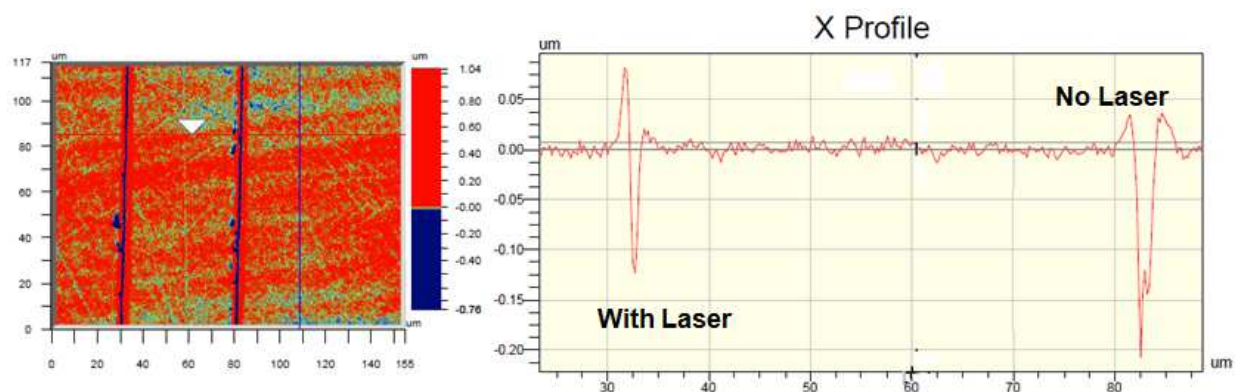


Fig. 7. Cross-section of scratches obtained from a white light interferometric profilometer

Fig. 8 shows the cross-section of the same two scratches (at a different point) taken at an equal thrust force of approximately 40mN. The DBT depth identified for the scratch performed with laser heating just before the point of fracture is approximately 240nm. At this load, the scratch performed with no laser heating shows signs of severe fracture. In comparison, the DBT depth of the scratch performed with laser heating was approximately 135nm greater than the DBT depth of the scratch performed without laser heating.

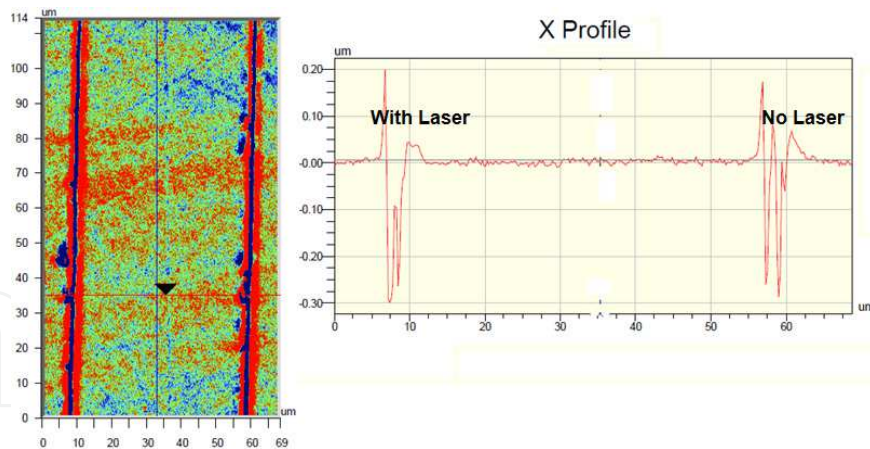


Fig. 8. Cross-section of scratches obtained from a white light interferometric profilometer

From Table 2, it is seen that the cut performed with laser heating yields a slightly higher cutting force at the DBT. This is due to the higher thrust force (40mN vs. 35mN) and larger depth of cut (240nm vs. 105nm).

Machining Condition	Thrust Force (Fz), (mN)	Cutting Force (Fx), (mN)	Depth of Cut(nm)	Scratch Nature
No Laser	30	10	95	Ductile
With Laser	30	10	145	Ductile
No Laser	35	12	105	DBT
With Laser	40	14	240	DBT

Table 2. Scratch test results

*Just before the DBT occurs.

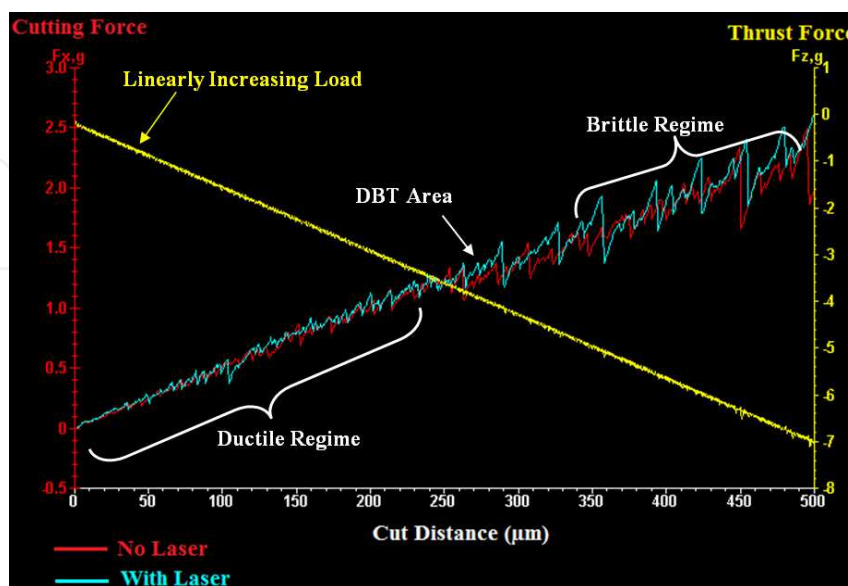


Fig. 8. Plot shows cutting force and thrust force data for both scratches

Analyzing the force data after the scratch experiments helps in correlating the onset of brittle fracture along the scratches. Brittle mode material removal is usually seen in the force data (especially cutting forces as it is more sensitive towards brittle fracture) and can be identified by its unstable behavior (higher standard deviation/ higher peaks-valleys in the force plots). Fig. 8 shows the force data plot obtained from both scratching conditions (with and without laser heating). Monitoring the cutting forces during the material removal process is also an effective in-situ method to detect the onset of brittle regime machining (onset of fracture occurrence).

3. Simulation Study of Thermal Effects for Analysis of Ductile Mode μ -LAM

This section of the chapter describes the numerical simulations of the ductile mode machining process conducted on single crystal 4H Silicon Carbide. The aim of the simulation work was to incorporate the laser heating effects in the simulation model to study the thermal softening behavior of SiC. In μ -LAM, a laser is used for heating the workpiece where the laser passes through the optically transparent diamond tool (Shayan et al., 2009). A laser source cannot be directly simulated in the simulation software hence thermal boundary conditions were defined on the tool and workpiece to mimic the laser heating effect. Initially, an approximate thermal softening curve was used to study the compatibility of the software (AdvantEdge from Third Wave Systems) with the desired laser heating and thermal softening effect (Virkar & Patten, 2009); i.e., a proof of concept. A new and more accurate thermal softening curve was developed based on references to incorporate more realistic thermal behavior (Virkar & Patten, 2010). The simulations were run at various temperatures throughout the thermal softening regime (up to the melting or decomposition point) and the changes in chip formation, cutting forces and pressures were studied.

3.1 FEM for μ -LAM Process

μ -LAM is a ductile mode material removal process developed for machining of nominally brittle materials augmented with thermal softening (provided by laser heating). Ductile mode machining implies plastic deformation and material removal, rather than brittle fracture, resulting in a smooth fracture free machined surface. This ductile mode material removal can be attributed to a High Pressure Phase Transformation (HPPT) at the tool-chip interface and the resultant high pressure phase is metallic or amorphous, and ductile. The HPPT occurs due to contact between the sharp tool and workpiece at or below critical depth of cut, i.e., the ductile to brittle transition. The recent work by (Patten et al., 2005) has determined the critical depth for ductile regime machining of single crystal SiC (Patten et al. 2005). These critical depths are in nano scale ($< 1 \mu\text{m}$) for SiC (Patten et al., 2004; Patten et al. 2005; Patten & Jacob, 2008).

Due to the metallic and ductile nature of the high pressure metallic phase that occurs at the tool chip interface, the metal machining software 'AdvantEdge' can be used to simulate the μ -LAM process and the scope of the work reported herein is limited to plastic deformation and ductile material removal. The software currently considers only ductile or plastic material removal and does not consider a fracture criterion or brittle material removing mechanisms. In the ductile mode, the software can be used to predict the forces and

pressures generated by the tool-chip interaction for a given set of process conditions and tool geometry, assuming an appropriate material model is used (Jacob, 2006). The material properties include elastic and plastic behavior, thermal softening, strain rate and heat transfer parameters.

The material model used in the current work is the Drucker-Prager model, which is used to accommodate the pressure induced phase transformation (pressure sensitivity) and the resultant elastic-plastic behavior (Ajarapu et al., 2004). The Drucker-Prager yield criterion is given by:

$$\sqrt{3J_2} + I_1\alpha - \kappa = 0 \quad (5)$$

Where I_1 is the first invariant of stress tensor and J_2 is the second invariant of deviatoric stress tensor, α is the Drucker-Prager coefficient and κ is the material constant.

The quantity I_1 is given by

$$I_1 = \sigma_1 + \sigma_2 + \sigma_3 \quad (6)$$

The quantity J_2 is given by

$$J_2 = 1/6 [(\alpha_1 - \alpha_2)^2 + (\alpha_2 - \alpha_3)^2 + (\alpha_3 - \alpha_1)^2] \quad (7)$$

where $\sigma_1, \sigma_2,$ and σ_3 are the principal stresses.

The quantity κ is given by

$$\kappa = \frac{2\sigma_c\sigma_t}{\sigma_c + \sigma_t} \quad (8)$$

which is equal to yield stress in the case when $\sigma_c = \sigma_t$, i.e. no pressure dependency, and where σ_c and σ_t are the yield stress in compression and tension respectively.

The hardness of the SiC material is 26 GPa and the initial yield stress is taken to be 11.82 GPa based on a proposed initial tensile yield (σ_t) value of $H/2.2$ for brittle materials (Gilman, 1975). The compressive yield (σ_c) is set to equal the hardness (H) of the material, to reflect the effect of the HPPT (Jacob, 2006; Ajarapu et al., 2004).

For uniaxial stress state (where σ_2 and σ_3 are zero), I_1 and J_2 are evaluated as:

$$I_1 = \sigma_1 \quad (9)$$

$$J_2 = \sigma_1^2/3 \quad (10)$$

Now using equation (5), κ equals 16.25 GPa while α equals -0.375. These parameters are essential to provide a pressure sensitive model.

3.2 Thermal Softening Behavior

The thermal softening function (AdvantEdge Manual, 2009) is defined as

$$\Theta(T) = c_0 + c_1T + c_2T^2 + c_3T^3 + c_4T^4 + c_5T^5 \quad \text{if } T < T_{cutoff} \quad (11)$$

$$\Theta(T) = \Theta(T_{cut}) \left(1 - \frac{T - T_{cut}}{T_{melt} - T_{cut}} \right) \quad \text{if } T \geq T_{cutoff} \quad (12)$$

The polynomial coefficients c_0 through c_5 are used fit to a 5th order polynomial, T is the temperature, T_{cutoff} is the linear cutoff temperature and T_{melt} is the melting temperature.

The initial work was started by using a simplified approximate thermal softening curve given below (Virkar & Patten, 2009).

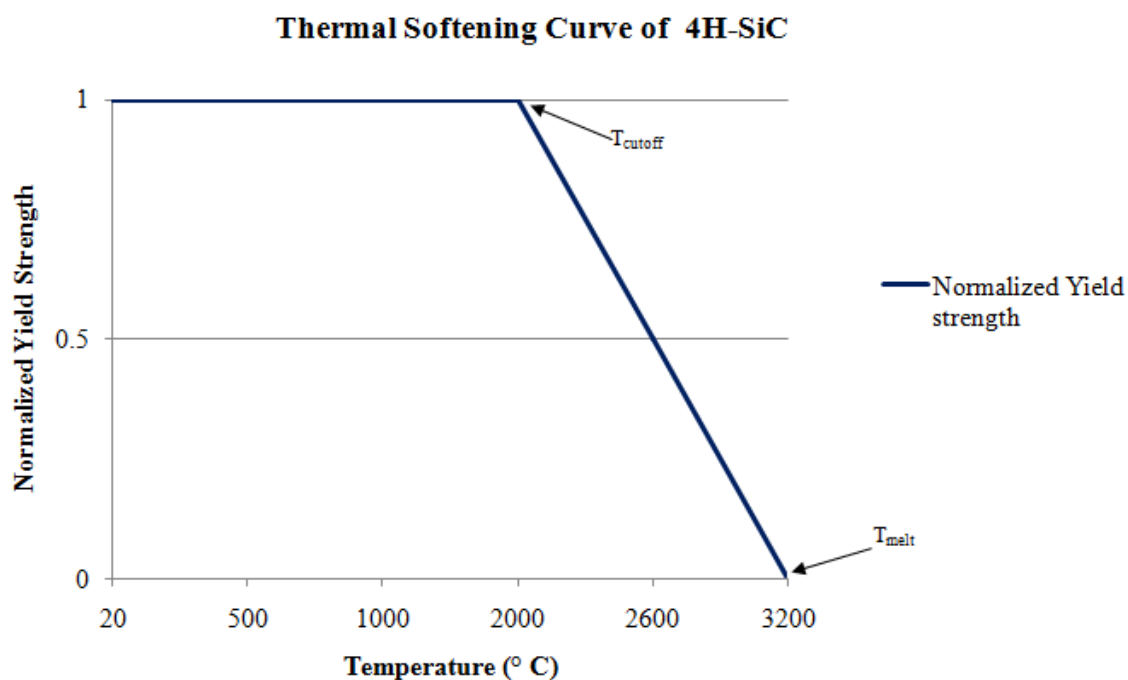


Fig. 9. Approximate thermal softening curve

In this curve, 2000° C and 3200° C were assumed as the thermal cutoff and melting temperature respectively. This model was used to test (evaluate) the thermal softening effect and to establish that it can be adequately incorporated in the simulation model (Virkar & Patten, 2009). For this curve, it is assumed that the yield strength remains constant from 20° C up to 2000° C and then it decreases linearly from 2000° C to the melting point (3200° C). Using polynomial equation (11) (Ajarapu et al., 2004), the constants c_0 to c_5 are made zero to get a straight line. This thermal softening curve was later modified by using the values of thermal softening and melting temperatures from literature references (Shim et al., 2008; Yonenaga, 2001; Yonenaga et al., 2000; Samant et al., 1998; Tsetkov et al., 1996; CREE material data sheet; Naylor et al., 1979). The new thermal softening curve is given below in Fig. 10, which will be the emphasis of the remainder of this section.

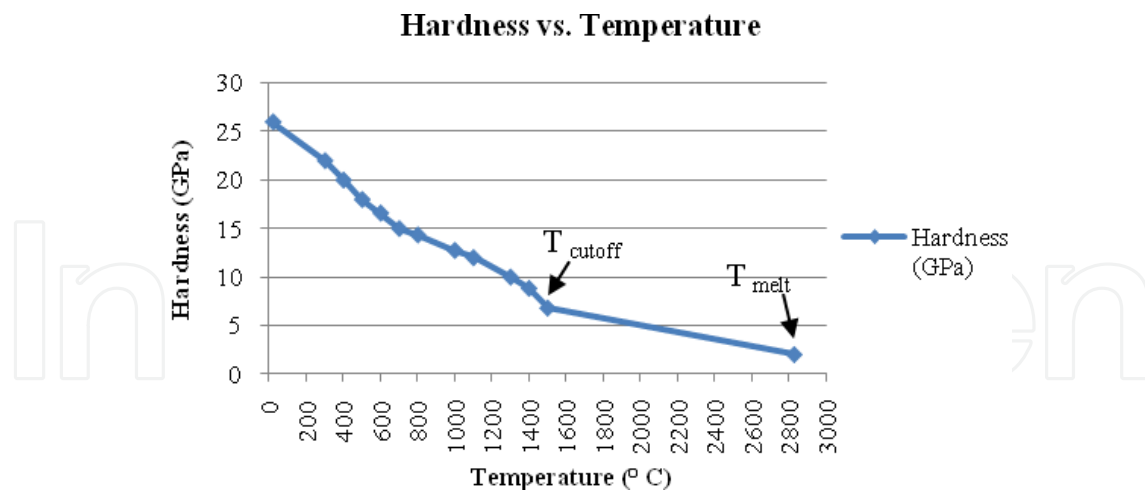


Fig. 10. Thermal Softening Curve based on references

Note: The temperature values T_{cutoff} and T_{melt} are estimated based on different values from various references (Shim et al., 2008; Yonenaga, 2001; Yonenaga et al., 2000; Samant et al., 1998; Tsetkov et al., 1996; CREE material data sheet; Naylor et al., 1979)

In this simulation work, a 3rd order polynomial curve was used to represent the thermal softening behavior. Using the polynomial equation (11), the constants c_0 to c_5 are assigned values based on the decrease in hardness values to get a 3rd order curve. Beyond the cutoff temperature, there is a linear decrease in the yield strength (there was no thermal softening values found in the literature over this range). This thermal softening curve demonstrates the thermal effects on SiC.

3.3 Tool and Workpiece Geometry and Properties

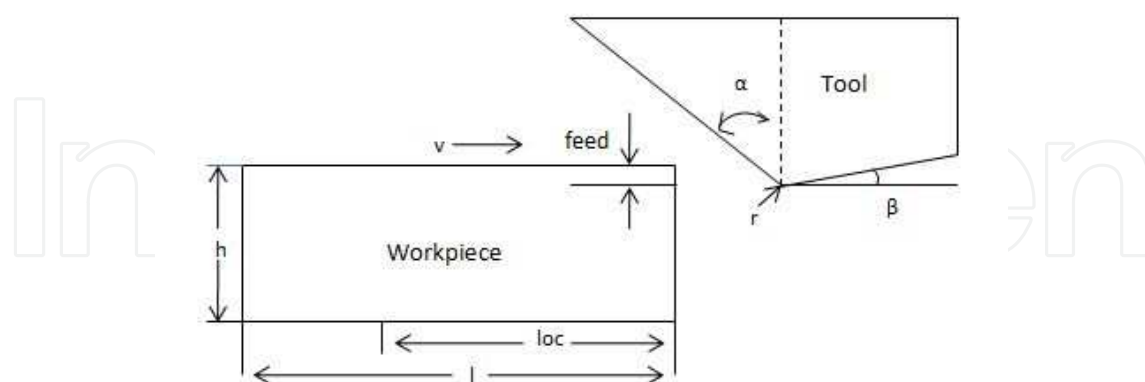


Fig. 11. Tool and Workpiece geometry

The workpiece was made long enough ($L = 0.08$ mm) to ensure that the length of cut (loc) would allow steady state conditions to be achieved during the simulation. The height ($h = 0.02$ mm) of the workpiece was much larger (between 10 to 100 times) in comparison to the feed (f) or uncut chip thickness (t) (Virkar & Patten, 2009; Virkar & Patten, 2010), which generally is between 50 and 500 nm. The boundary conditions of the workpiece surface are

assumed to be traction free and constrained in the vertical direction. The workpiece material properties (Refer Table 3) used in the simulation model are given below

Material properties	Value	Units
Elastic Modulus, E	330	GPa
Poisson's ratio	0.212	-
Hardness, H	26	GPa
Initial yield stress, σ_0 or κ	16.25	GPa
Reference plastic strain, ϵ_0^p	0.049	-
Drucker-Prager coefficient (DPO)	-0.375	-
Thermal Cutoff temperature	1500	° C
Melting temperature	2830	° C

Table 3. Workpiece material properties

The tool used in the simulation is a single point diamond. The tool geometry is given in Table 4. The simulations were conducted in 2-D and as a result a round nose tool geometry could not be simulated, therefore the simulated tool cutting edge is flat, with a width (depth) of 20 μm (0.02 mm). The top and back surfaces of the tool are fixed with adiabatic conditions.

Cutting Edge Radius, r, (nm)	100
Rake angle, α	- 45°
Relief angle, β	5°
Width of tool (μm)	20
Thermal Conductivity, W/m °C	1500
Heat Capacity, J/kg °C	471.5
Density, kg/m ³	3520
Elastic Modulus, GPa	1050
Poisson's ratio	0.2

Table 4. Tool Geometry and material properties

The -45° rake angle creates a high pressure (compression) sufficient to accommodate the HPPT, thus the chip formation zone is conducive for ductile deformation (Patten et al., 2005).

3.4 Simulation Model

The simulation method is based upon a 2-D Lagrangian finite-element machining model assuming plane strain conditions (AdvantEdge Manual, 2009). The simulations were carried

out by specifying the material properties for 4H-SiC. The constitutive model does not incorporate crystallographic planes/orientations and treats the material as elastic-plastic and ductile. To reflect the ductile behavior in ceramics, promoted by the HPPT, a pressure sensitive Drucker-Prager constitutive model is used (Patten et al., 2004; Patten et al., 2005).

The objective of this work was to incorporate the thermal effects that would closely replicate the actual heating conditions during the μ -LAM process. The software cannot directly incorporate the laser heating source in the model hence thermal boundary conditions similar to the laser heating effect are defined. The thermal effects were simulated by defining thermal boundary conditions in three different ways to capture the essence of the laser heating effect. In the first case a thermal boundary condition was provided on the tool tip about $\sim 2\mu\text{m}$ along the rake and clearance faces away from the cutting edge (Refer Fig. 12).

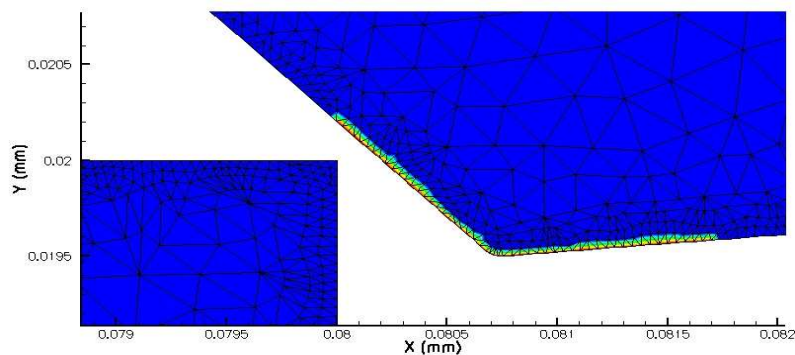


Fig. 12. Tooltip Boundary Condition

The blue color contour identifies the tool and workpiece being at room temperature and at the tool tip, the contour color varies which is due to a thermal boundary defined for heating effect. The temperature of the thermal boundary would be similar to the temperature of laser heating during machining. In the second case, the entire rake and clearance face of the tool was heated. In Fig. 4, the thermal boundary is at the tool tip but for the second case the thermal boundary was defined such that it extended on the entire rake and clearance face. For the third case, a thermal boundary was provided on the workpiece top surface (Refer Fig. 13) to reflect the heating effect of the laser on the workpiece surface. Note in the initial work (Virkar & Patten, 2009), the entire tool and workpiece system was uniformly heated to the elevated temperatures instead of a boundary condition.

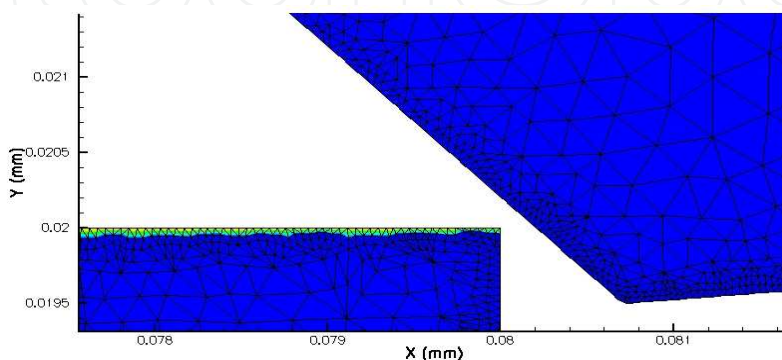


Fig. 13. Workpiece Boundary Condition

The process parameters are given in Table 5

Parameters	Values
Feed (nm)	500
Coefficient of friction	0.3
Cutting speed (m/s)	1
Depth (width) of cut (mm)	0.02

Table 5. Process Parameters

The simulations were conducted with the values given in Tables 3, 4, and 5. The feed in the 2-D simulation relates to the uncut chip thickness, and the depth of cut refers to the workpiece width. With the given values of high negative rake angle and small feed, ductile mode machining is achieved (Jacob, 2006). The coefficient of friction was taken as 0.3, however the results are not very sensitive to this value (AdvantEdge Manual, 2009).

The simulation results include the cutting and thrust forces that are used for comparison to evaluate the various machining conditions (primarily the workpiece temperature and the resultant thermal softening effect). The simulations were carried out at various temperatures: 20° C, 700° C, 1500° C, 2200° C, and 2700° C where 1500° C is the thermal cutoff temperature as shown in Fig. 2. Beyond the thermal cutoff temperature, there is a linear decrease in the material strength until it reaches the melting point (2830° C). The results of the simulations were viewed in the post processing tool Tecplot (AdvantEdge Manual, 2009), which provides temperature, pressure, stress and strain contours along with the cutting and thrust force plots for analysis of the simulation results. At each of the simulated temperatures, the chip formation, force plots and pressure contours are used and compared to evaluate the results.

3.5 Analysis of Force Data

The cutting force data from the simulation output is used for calculating the approximate cutting pressures at the tool chip interface. The other parameters used are width of the tool and feed or uncut chip thickness to determine the uncut chip cross sectional area. The formula used is given below

$$\text{Cutting Pressure} = \frac{\text{Cutting Force } (F_c)}{\text{Chip Area } (A_c)} \quad (8)$$

The chip area is calculated by multiplying the width of the tool (20 μm) with programmed feed (0.5 μm) of the simulation. To generate a ductile cutting environment through applied stresses (hydrostatic and shear) requires that the pressures at the workpiece-chip interface be equal to, or greater than, the hardness of the material, which is taken as 26 GPa (i.e. the compressive yield) for 4H-SiC. The thermal softening effect results in decreasing cutting pressures as the simulation temperature increases. In μ-LAM the cutting pressures are lowered at the tool-chip interface due to thermal softening (Virkar & Patten, 2009). Tool wear is reduced due to the lower cutting forces and pressures.

3.6 Simulation Results

3.6.1 Tool Tip Boundary Condition

A thermal boundary is provided at the tip of the tool, $\sim 2 \mu\text{m}$ from the cutting edge, along the surface of the rake and clearance faces. During the actual $\mu\text{-LAM}$ process, the laser beam passes through the tip (cutting edge) of the tool, is absorbed by the workpiece and results in the heating of the workpiece locally at the tool-workpiece interface. Hence, this boundary condition (on the cutting edge, $\sim 2\mu\text{m}$ along the rake and clearance faces) is a very close approximation to the actual location of the heating source in the actual $\mu\text{-LAM}$ process (note that it is on the wrong surface however, located on the tool rather than the workpiece). Table 6 summarizes the simulation results, where the heating effect is implemented on the tool rather than on the workpiece and then the heat is conducted to the workpiece at the tool-workpiece interface.

Temperatures ($^{\circ}\text{C}$)	Cutting Force (mN)	Thrust Force (mN)	Chip formation	Pressure (GPa)
20	500	900	Yes	50
700	460	890	No	46
1500	370	610	No	37
2200	200	300	No	20
2700	80	130	Yes	8

Table 6. Tooltip Boundary Condition Results

In this case, the chip formation is seen at 20°C and 2700°C (Refer Table 6) and for the rest of the temperature points there is a smooth ductile material deformation (pile up and plowing in front of the tool), but no chip formation.

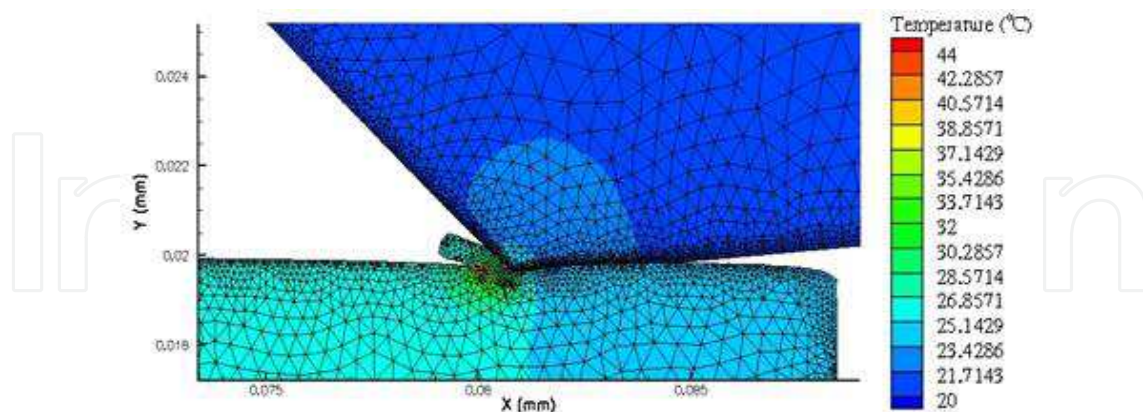


Fig. 14. At 20°C

The chip formation at 2700°C (Fig. 7) is quite different than that at 20°C (Refer Fig. 8) as the chip is very thick at the base and pointed at its end in the former case.

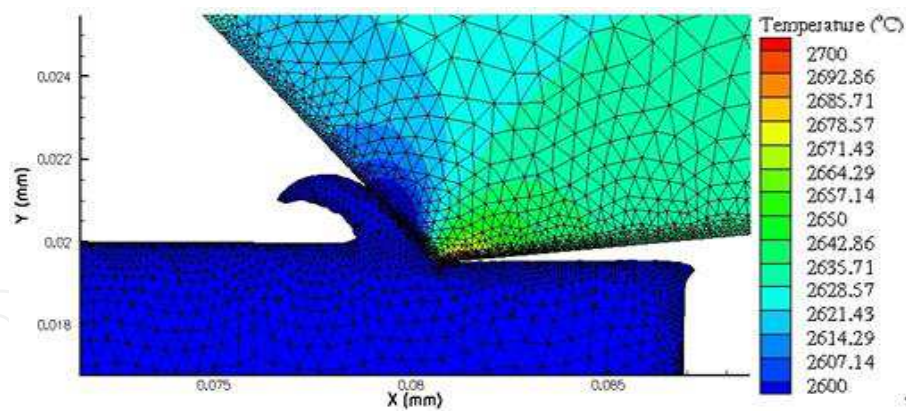


Fig. 15. At 2700° C

Figs. 16 and 17 describe the response of force and cutting pressure with respect to the temperature. The cutting pressure is above the hardness value (26 GPa) at 1500° C which means that the workpiece is still retaining its strength. Above 1500° C the pressure drops below the hardness value (Refer Table 6). The cutting forces and pressures show a decreasing trend with increase in temperature, as expected (Refer Fig. 16 and 17).

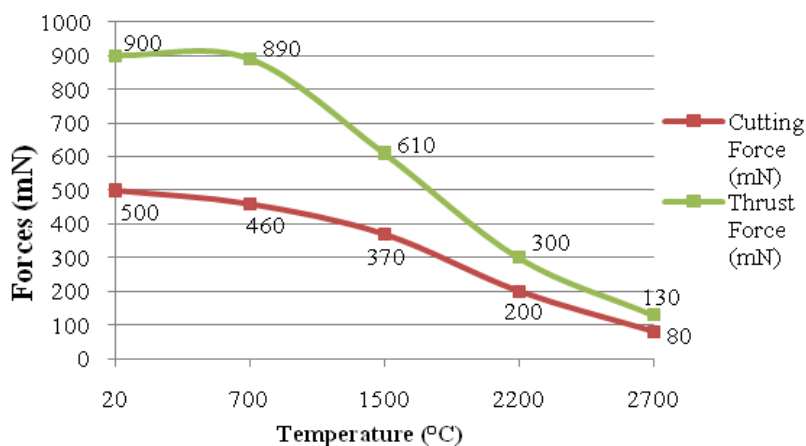


Fig. 16. Forces vs. Temperature curve

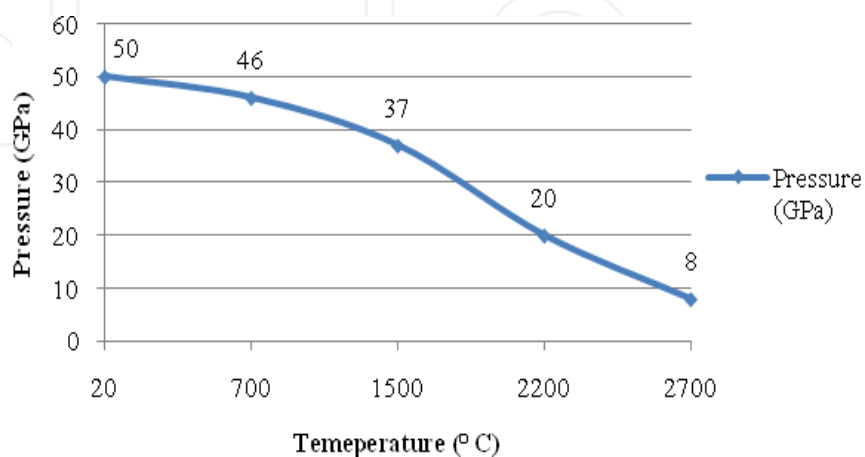


Fig. 17. Cutting Pressure vs. Temperature

3.6.2 Rake and Clearance Face heated Boundary Condition

In this case, a thermal boundary condition was defined on the entire rake and clearance face. This case was the first condition to start with this study and the easiest boundary condition to implement on the tool. Using this boundary condition, the effect on chip formation and cutting forces and pressures was established. Table 7 summarizes the result details:

Temperatures (° C)	Cutting Force (mN)	Thrust Force (mN)	Chip formation	Pressure (GPa)
20	500	1060	Yes	50
700	450	1000	No	45
1500	380	620	No	38
2200	200	300	No	20
2700	60	90	Yes	6

Table 7. Tool Rake and Clearance face Boundary Condition Results

In this case, the chip formation was again seen at 20° C and 2700° C (Refer Table 7). This behavior is also seen in the tooltip boundary condition (Refer Table 4). At 2700° C the chip formed was thicker as compared to the chip at 20° C (Refer Figs. 18 and 19)

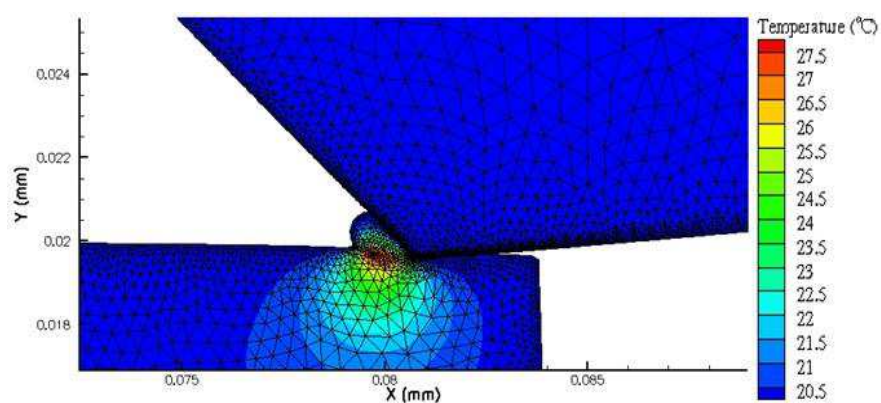


Fig. 18. At 20° C

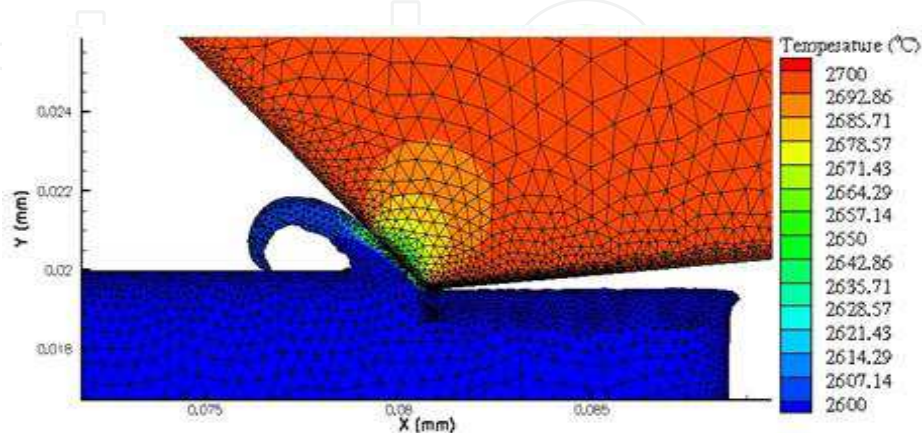


Fig. 19. At 2700° C

Figs. 20 and 21 shows a decreasing trend in the cutting forces and pressures with an increase in temperature.

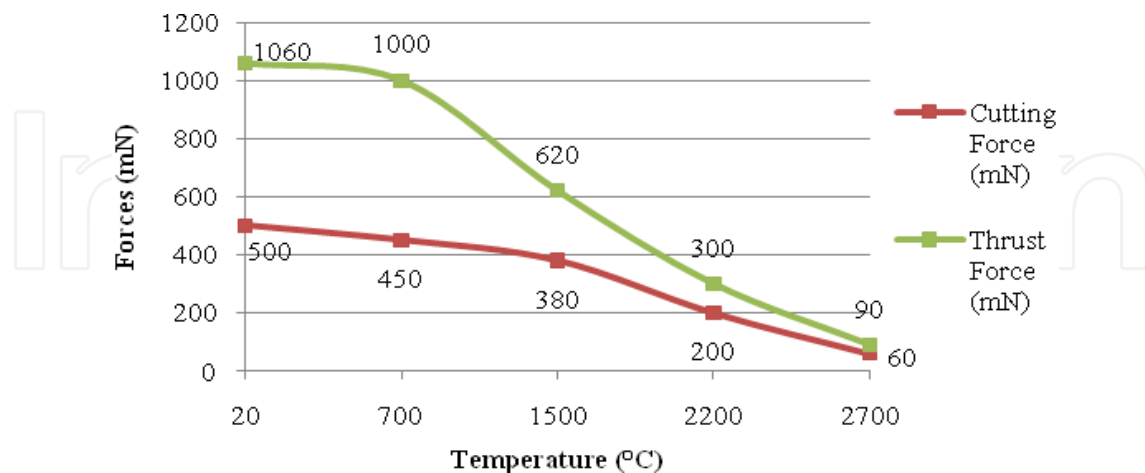


Fig. 20. Forces vs. Temperature curve

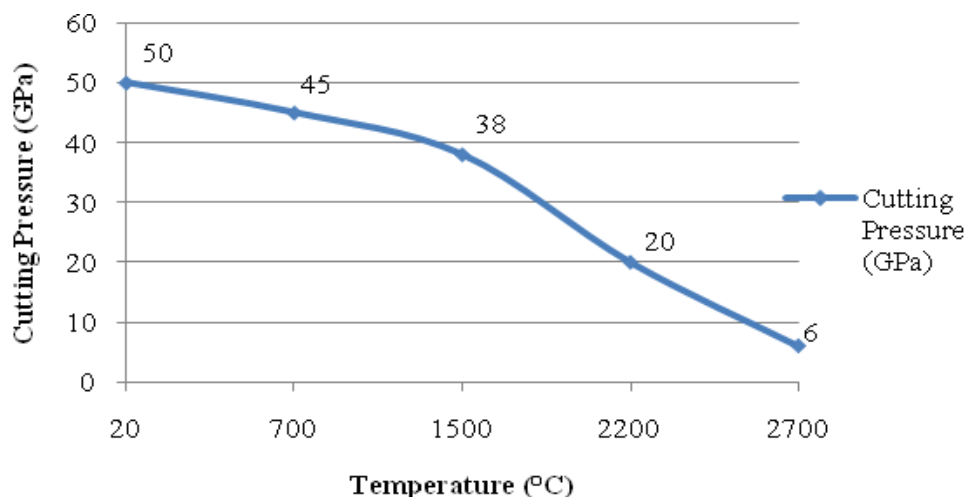


Fig. 21. Cutting Pressure vs. Temperature

3.6.3 Workpiece Boundary Condition

In this case, a thermal boundary is provided on the top surface of the workpiece. In μ -LAM, the workpiece surface is directly heated by a laser (the workpiece absorbs the laser energy and is subsequently heated), which passes through the tool hence the workpiece boundary condition closely replicates the actual process, i.e., the workpiece is directly heated. This phenomena is not quite directly comparable with the experiments as in μ -LAM process just the area under the tool tip (tool workpiece interface) is heated (based upon the laser spot size) Table 8 summarizes the simulation results.

Temperatures (° C)	Cutting Force (mN)	Thrust Force (mN)	Chip formation	Pressure (GPa)
20	470	1040	Yes	47
700	450	950	No	45
1500	390	570	No	39
2200	200	260	No	20
2700	30	40	No	3

Table 8. Workpiece Boundary Condition Results

(Note that the temperature scale is changed in the above figures to more clearly show the thermal effect)

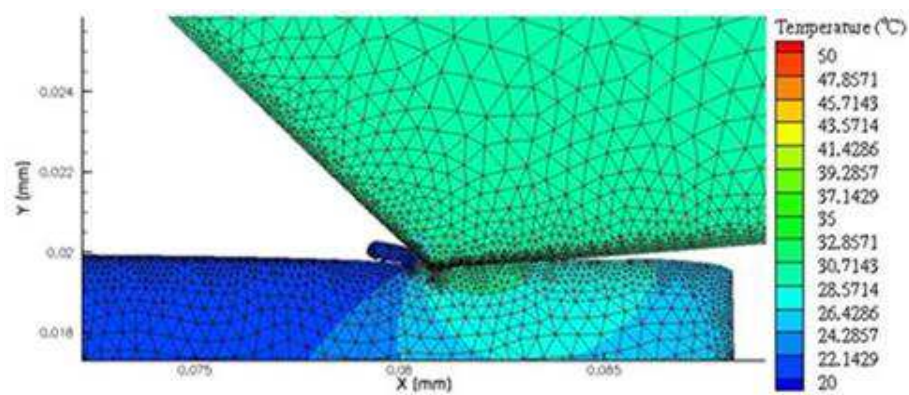


Fig. 22. At 20° C

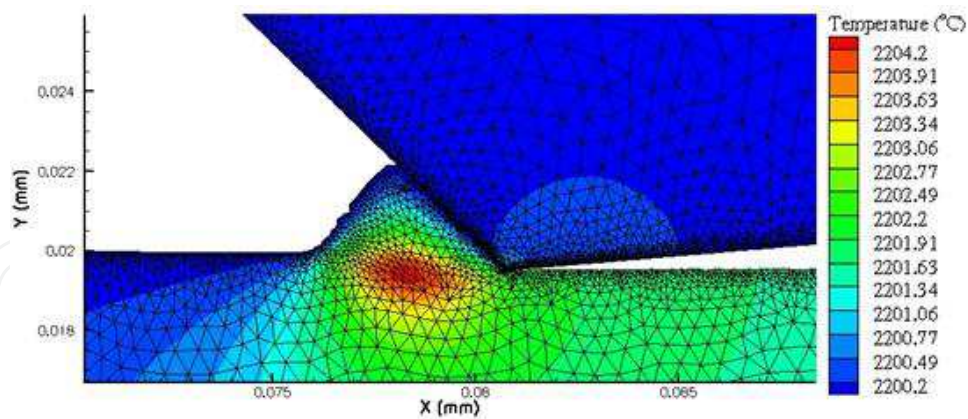


Fig. 23. At 2200° C

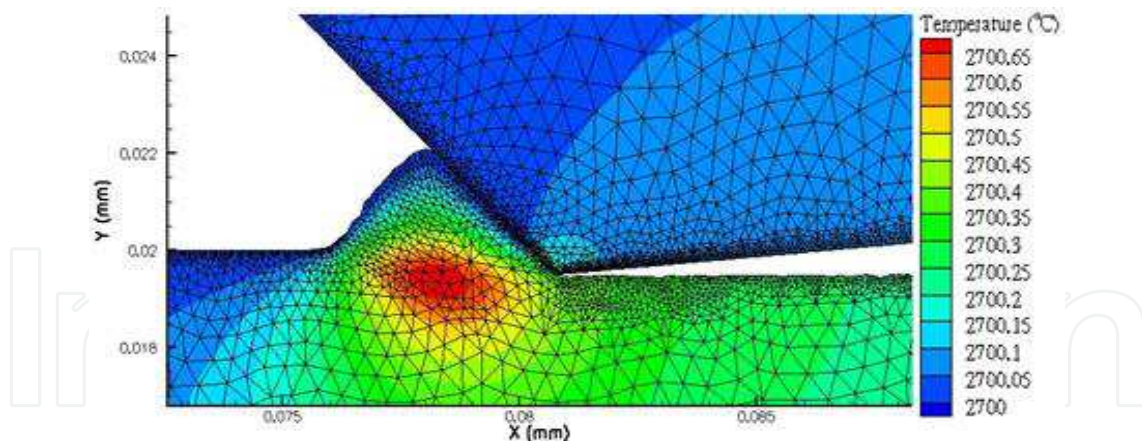


Fig. 24. (At 2700^o C)

In this case, the actual chip formation is seen only at 20° C. There is no chip formation seen at other temperature points (Refer to Table 8). The material deformation in this case is seen in Fig. 22, 23 and 24 (Note that the temperature scale is changed in both figures to show and highlight the thermal effect). The cutting forces and pressures show a decreasing trend (Refer Fig. 25 and 26) with increase in temperature which is an indication of thermal softening.

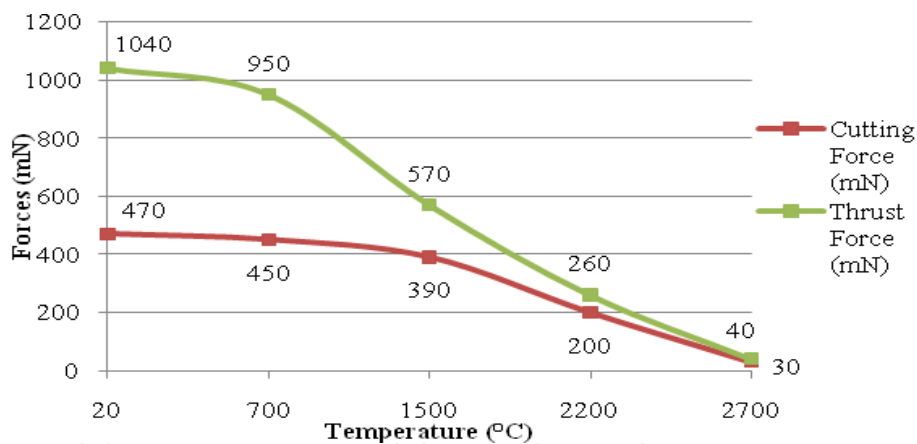


Fig. 25. Forces vs. Temperature curve

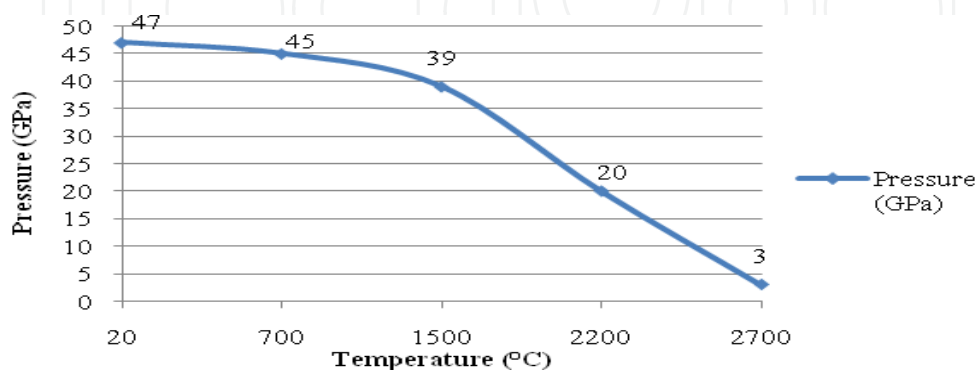


Fig. 26. Cutting Pressure vs. Temperature

3.7 Interaction between Stress and Temperature in μ -LAM

This interaction study between stress and temperature is developed from the simulation results (Virkar & Patten, 2010). The results for workpiece and tool-tip boundary conditions were considered for the analysis. The temperature dependence is determined from the yield strength vs. temperature curve given in Table 9 (this figure is similar for Fig. 10, Hardness vs. Temperature). The yield strength for brittle materials like SiC is calculated using $H/2.2$ (Gilman, 1975), where H is hardness value of SiC. The H value is derived from the hardness vs. temperature curve given in Fig. 10. The hardness values and the corresponding yield strength values are given in Table 7.

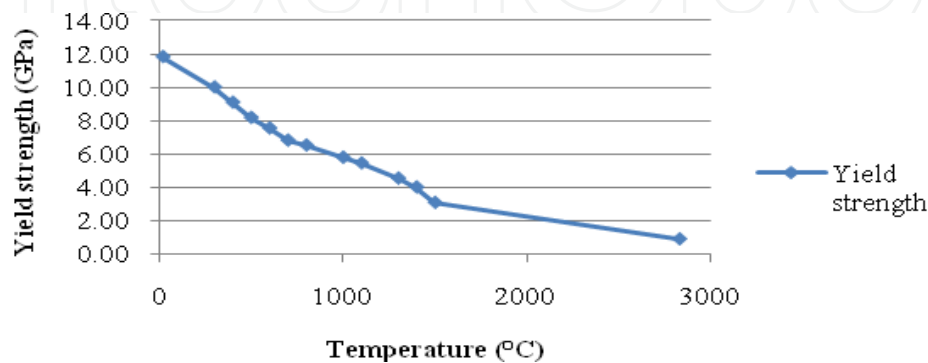


Fig. 27. Yield strength vs. temperature curve

Note: The yield strength in above figure refers to estimated tensile yield strength

Temperature (°C)	Hardness, (σ_c) GPa	Yield strength, (σ_t) GPa
20	26	11.82
300	22	10.00
400	20	9.09
500	18	8.18
600	16.6	7.55
700	15	6.82
800	14.35	6.52
1000	12.75	5.80
1100	12	5.45
1300	10	4.55
1400	8.835	4.02
1500	6.8	3.09
2830	2	0.91

Table 9. Yield strength as a function of temperature

Two approaches were selected for analyzing the interaction between the stress and temperature namely,

1. Normalized Cutting Force Approach
2. Yield strength as a function of pressure and temperature

3.7.1 Normalized Cutting Force approach

An approximate equation for cutting energy was developed using the cutting forces from the simulation at selected temperature points in the thermal softening regime (Virkar & Patten, 2010). The equation is given as

$$\text{Normalized Cutting Force} = X \text{ stress} + Y \text{ temperature} \quad (9)$$

where X and Y are proportional multipliers and $X + Y = 100\%$.

The Normalized cutting force is obtained from the cutting forces taken directly from the simulation output (Refer Table 6) at each designated temperature point and dividing them by the force at 20° C. The stress factor in the equation is substituted as 1 because in the Drucker-Prager model stress or yield is not a function of temperature. The thermal (temperature) contribution is the tensile yield strength value taken from the yield strength vs. temperature curve (Refer Fig. 27) at the designated simulation temperature. In this way the percentage interaction or contribution of stress and temperature is determined for all boundary condition simulations given in Table 10.

	Temperatures (° C)	Stress %	Temperature %
Tooltip Boundary Condition simulation	20	100	0
	700	80.95	19.05
	1500	64.86	35.14
	2200	26.83	73.17
	2700	6.67	93.33
Workpiece Boundary Condition simulation	20	100	0
	700	76.19	23.81
	1500	59.52	40.48
	2200	26	74
	2700	4	96

Table 10. Percentage interaction of stress and temperature

From this approach it is seen that for both the boundary conditions at 20° C, the stress contribution dominated (no thermal effect). As the temperature of the boundary condition increases the temperature contribution increases reducing the effect due to stress contribution. The cutting and thrust forces decrease as the temperature contribution increases thus showing the thermal softening effect. The apparent crossover in contribution of stress to temperature occurs between 1500° C to 2200° C.

3.7.2 Yield strength as a function of pressure and temperature approach

This approach is based on the Drucker-Prager yield criterion. At first, the tensile yield strength was calculated as a function of temperature (Refer Table 11). In the Drucker-Prager model, the κ value is the calculated yield which is determined using equation (8). The σ_c is taken as the room temperature hardness of SiC, which is kept constant and σ_t is the tensile yield which is substituted from the yield strength vs. temperature curve (Refer Fig. 27). The calculated yield (κ) from 20° C until 2830° C is calculated using the equation (8) and is given in Table 11:

Temperature (°C)	Hardness, (σ_c) GPa	Tensile Yield strength, (σ_t) - GPa	Calculated yield with constant σ_c - GPa
20	26	11.82	16.25
300	22	10.00	14.44
400	20	9.09	13.47
500	18	8.18	12.45
600	16.6	7.55	11.70
700	15	6.82	10.80
800	14.35	6.52	10.43
1000	12.75	5.80	9.48
1100	12	5.45	9.02
1300	10	4.55	7.74
1400	8.835	4.02	6.96
1500	6.8	3.09	5.53
2830	2	0.91	1.76

Table 11. Calculated yield strength as a function of temperature

Note: The initial compressive yield σ_c is kept constant to see the effect due to pressure without any thermal effect as we assume it to be equal to the hardness previously.

From Table 11 we can see that the yield strength goes on decreasing as the temperature of the simulation is increasing. The data for hardness vs. temperature is limited only up until 1500° C based on the references. From 1500° C upto 2830° C, the hardness vs. temperature is approximate and hence there is a linear decrease in the yield strength (Fig. 2). Hence the σ_t value at 2200° C is based on interpolation between 1500° C and 2830° C on the temperature scale.

To calculate the yield strength as a function of pressure, we consider the Drucker-Prager yield criterion from equation (5). In that equation, I_1 and J_2 are the invariants of stress tensors and are dependent on the three dimensional stresses which are taken from the simulation output. By substituting the values of σ_1 , σ_2 , σ_3 in equations (6) and (7), we get value of I_1 and J_2 . Substituting these values back into equation (5) gives us the value of calculated yield κ . The value of Drucker-Prager coefficient (α) is kept constant at 0.375 which is obtained assuming plain strain conditions. Table 12 shows all the calculated values.

From Simulation					Calculated Values			
Boundary Condition	Temp. (° C)	σ_x (GPa)	σ_y (GPa)	σ_z (GPa)	I_1 (GPa)	J_2 (GPa)	K (GPa)	Max. pressure (GPa)
WBC	20	38.74	25.92	32.41	97.06	41.08	47.50	50.00
WBC	700	22.06	21.62	21.97	65.65	0.05	25.02	46.00
WBC	1500	8.86	10.79	9.81	29.46	0.94	12.72	37.00
WBC	2200	4.78	2.58	3.68	11.03	1.21	6.04	20.00
WBC	2700	0.40	0.78	0.59	1.77	0.04	0.99	8.00
Tooltip	20	35.12	24.53	29.80	89.45	28.06	42.71	47.00
Tooltip	700	31.55	14.27	22.86	68.67	74.63	40.71	45.00
Tooltip	1500	16.28	12.65	14.71	43.64	3.31	19.51	39.00
Tooltip	2200	10.07	6.51	8.29	24.87	3.17	12.41	20.00
Tooltip	2700	4.41	4.08	4.25	12.74	0.03	5.06	3.00

Table 12. Yield strength as a function of pressure

From Table 12, we can see that the calculated yield goes down with increase in temperature. This effect is seen as the σ_t factor in Drucker-Prager model is affected by temperature. There is also a column of maximum pressure which is calculated by dividing the cutting forces by cross sectional area of contact surface of tool. Thus, by both approaches the same trend is seen in the behavior of SiC. As the temperature goes on increasing the dominance due to stress reduces.

4. Conclusion

For the experimental study, micro-laser assisted scratch tests were successful in demonstrating the enhanced thermal softening of the material resulting in a greater ductile to brittle transition depth. Laser heating was successfully demonstrated as evidenced by the significant increase in the ductile response of single crystal 4H-Silicon Carbide in the {1010} plane along the <1010> direction. Laser assisted (heating, thermal softening and reduced brittleness) material removal resulted in greater depths of cuts (in the ductile regime) at less applied thrust forces, smaller cutting forces and a larger critical DoC. Force analysis (thrust and cutting), optical microscopy and white light interferometry served as useful analysis methods to detect the enhanced ductile response and reduced brittle fracture as a result of preferential material heating (of the high pressure phase transformed material). Results obtained from this study are promising to further implement micro-laser assisted machining (μ -LAM) in operations such as single point diamond turning. Lower cutting forces obtained from the μ -LAM process are favorable to minimize tool wear while machining abrasive ceramics/semiconductors such as Quartz, Silicon and Silicon Carbide. The results from this study also will benefit the manufacture of brittle materials as laser heating is proven to decrease the brittle response in ceramics and semiconductors which can result in higher productivity rates (i.e. higher material removal rate).

For the simulation study, a set of carefully designed thermal boundary conditions were simulated in 2D using the software TWS AdvantEdge software. The simulations were used to predict the thermal softening behavior of SiC using the Drucker-Prager yield criterion. In the results of each of the cases, there is a decreasing trend in cutting forces and pressures with an increase in temperature. This confirms the thermal softening behavior due to simulated laser heating, which reduces the hardness of the material. The interaction between stress and temperature was also determined from the boundary condition simulation outputs. It showed that the dominance of stress decreases with increase in temperature.

5. Future Research

The results and data obtained will be implemented in establishing machining parameters to perform ductile mode micro-laser assisted single point diamond turning (SPDT) on SiC. Various scratch tests are currently being conducted to establish optimized correlation between laser power and machining parameters such as depth of cut, feed and cutting speed.

High pressure and temperature experiments have been studied (and currently under analysis) to determine the pressure-temperature correlation with the phase transition during the μ -LAM process using laser heated diamond anvil cells (DAC). This analysis however neglects the effect due to shear forces (which is believed to contribute significantly in the phase transformation of SiC). To include shear force analysis, a new DAC is being developed that will account for the missing shear component in a regular DAC cell. Furthermore, the change in lattice volume will be calculated and the cell structure of the newly developed high pressure phase material will be determined. Laser absorption measurements are also being conducted on the current high pressure phase samples to optimize the laser power during the μ -LAM process.

6. Acknowledgements

The authors would like to thank Husyein Bogac Poyraz for his contribution in the experiments and Third Wave Systems (TWS) Inc., for their generous support and technical assistance. The authors are also thankful to the National Science Foundation (NSF) for their grant CMMI-0757339.

7. References

- AdvantEdge User Manual, version 5.3, 2009
- Ajjarapu, S.K.; Cherukuri, H.; Patten, J.A.; Brand, C.J. (2004). Numerical simulations of ductile regime machining of Silicon Nitride using Drager-Prager model, *Proc. Institute of Mechanical Engineers*, 218(C), pp. 1-6
- Ashurst, W.R.; Wijesundara, M.B.J.; Carraro, C. & Maboudian, R. (2004). Tribological impact of SiC coating on released polysilicon structures, *Tribol. Lett.*, Vol.17, No.2, pp. 195-198
- Bifano, T.G.; Dow, T.G. & Scattergood, R.O. (1991). Ductile regime grinding- a new technology for machining brittle materials, *Journal of Engineering for Industry*, Vol.113, pp. 184-189

- Blake, P.N. & Scattergood, R.O. (1990). Ductile-regime machining of germanium and silicon, *Journal of the American Ceramic Society*, Vol.73, Issue 4, pp 949-957
- Blake, P.N. & Scattergood, R.O. (1990). Precision machining of ceramic materials, *Journal of the American Ceramic Society*, Vol.73, No.4, pp. 949-957
- Blackley, W.S. & Scattergood, R.O. (1994). Chip topography for ductile-regime machining for germanium, *Journal of Engineering for Industry*, Vol.116, pp. 263-266
- CREE material data sheet <http://www.cree.com/products/pdf/MAT-CATALOG.pdf>
- Dong, L. & Patten, J.A. (2007). Real time infrared (IR) thermal imaging of laser-heated high pressure phase of silicon, *Advanced Laser Applications Conference & Expo (ALAC 2007)*, Boston, MA.
- Dong, L. (2006). In-situ detection and heating of high pressure metallic phase of silicon during scratching, *PhD dissertation, University of North Carolina at Charlotte*
- Gao, D; Wijesundara, M.B.J.; Carraro, C.; Low, C.W.; Howe, R.T. & Maboudian, R. (2003). High modulus polycrystalline 3C-SiC technology for RF MEMS, *Proc. Transducers 12th Int. conf. Solid-State Sensors and Actuators*, pp. 1160-1163
- Gilman J.J. (1975). Relationship between impact yield stress and indentation hardness, *Journal of Applied Physics*, 46(4), pp. 1435-1436
- Jahanmir, S; Ives, L.K.; Ruff, A.W. & Peterson, M.B. (1992). Ceramic machining: assessment of current practice and research needs in the United States, *NIST Special Publication*, Vol. 834, p.102
- Leung, T.P.; Lee, W.B. & Lu, X.M. (1998). Diamond turning of silicon substrates in ductile-regime, *Journal of Materials Processing Technology*, Vol.73, pp. 42-48
- Marusich, T.D.; Askari, E. (2001). Modelling residual stress and workpiece surfaces in machined surfaces, www.thirdwavesys.com
- Morris, J.C.; Callahan, D.L.; Kulik, J.; Patten, J.A. & Scattergood, R.O. (1995). Origins of the ductile regime in single-point diamond turning of semiconductors, *Journal of American Ceramic Society*, Vol.78, No.8, pp. 2015-2020
- Morris, J.C.; Callahan, D.L.; Kulik; Patten, J.; & Scattergood, R.O. (1995). Origins of the ductile regime in single point diamond turning of semiconductors, *Journal of American Ceramic Society*, Vol.78, No.6, pp. 2015-2020
- Naylor, M.G.; Page, T.F. (1979). The effect of temperature and load on the indentation hardness behavior of Silicon Carbide engineering ceramics, *Proceedings of International Conference on erosion of soil and impact*, pp. 32
- Jacob, J. (2006). Numerical simulation on machining of silicon carbide, *Master's Thesis*, Western Michigan University, MI, USA
- O'Connor, B.; Marsh, E.; Couey, J. (2005). On the effect of crystallographic orientations for ductile material removal in Silicon, *Precision Engineering*, Vol. 29(1), pp. 124-132
- Patten, J.A.; Bhattacharya, B. (2006). Single point diamond turning of CVD coated silicon carbide, *Journal of Manufacturing Science- ASME*, Vol. 127, pp. 522
- Patten, J.A.; Cherukuri, H.; Yan, J.W. (2004). Ductile regime machining of semiconductors and ceramics, *Institute of Physics Publishing*, pp. 661
- Patten, J.A.; Fesperman, R.; Kumar, S.; McSpadden, S.; Qu, J.; Lance, M.; Nemanich, R. & Huening, J. (2003). "High-Pressure Phase Transformation of Silicon Nitride", *Applied Physics Letters*, 83(23), 4740-4742, 2003.
- Patten, J.A.; Gao, W. & Yasuto, K. (2005). Ductile regime nanomachining of single-crystal silicon carbide, *Journal of Manufacturing Science- ASME*, Vol.127, No.3, pp. 522-532

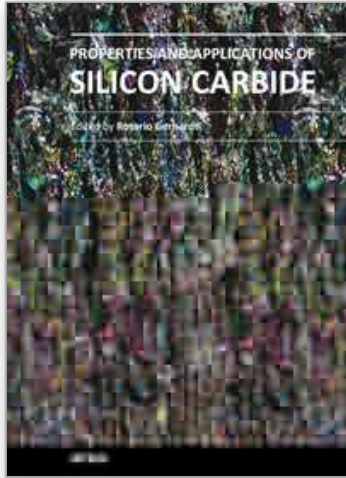
- Patten, J.A.; Jacob, J. (2008). Comparison between numerical simulations and experiments for single point diamond turning of single crystal silicon carbide, *Journal of Manufacturing Processes*, Vol. 10, pp. 28-33
- Patten, J.A.; Jacob, J.; Bhattacharya, B.; Grevstad, A. (2008). Comparison between numerical simulation and experiments for single point diamond turning of Silicon Carbide, *Society of Manufacturing Engineers NAMRAC conference*, pp.2
- Ravindra, D; Patten, J. & Tano, M. (2007). Ductile to brittle transition in a single crystal 4H SiC by performing nanometric machining, *Proc. ISAAT 2007 Precision Grinding and Abrasive Technology at SME International Grinding Conference, Advances in Abrasive Technology*, X, pp 459-465
- Rebro, P.A.; Pfefferkorn, F.E.; Shin, Y.C. & Incropera, F.P. (2002). Comparative assessment of laser-assisted machining of various ceramics, *Transactions of NAMRI*, Vol.30, pp. 153-160
- Ravindra, D.; Patten, J. & Qu, J. (2009). Single point diamond turning effects on surface quality and subsurface damage in ceramics, *Proceedings of the ASME International Manufacturing Science and Engineering Conference*, West Lafayette, IN.
- Ravindra, D. & Patten, J. (2008). Improving the surface roughness of a CVD coated SiC disk by performing ductile regime single point diamond turning, *Proceedings of the ASME International Manufacturing Science and Engineering Conference*, Evanston, IL.
- Samant, A.V.; Zhou, W.L.; Pirouz, P. (1998). Effect of test temperature and strain rate on the yield strength of monocrystalline 6H-SiC, *Physica Status Solidi (a)*, Vol. 166, pp. 155
- Shayan, A.R.; Poyraz, H.B.; Ravindra, D.; Ghantasala, M. & Patten, J.A. (2009). Force analysis, mechanical energy and laser heating evaluation of scratch tests on silicon carbide (4H-SiC) in micro-laser assisted machining (μ -LAM) process, *Proceedings of the ASME International Manufacturing Science and Engineering Conference*, Evanston, IL.
- Shayan, A.R.; Poyraz, H. B.; Ravindra, D. & Patten, J.A. (2009). Pressure and temperature effects in micro-laser assisted machining (μ -LAM) of silicon carbide, *Transactions NAMRI/SME*, Vol.37, pp. 75-80
- Shim, S.; Jang, J.I., Pharr, G. M. (2008). Extraction of flow properties of single crystal Silicon Carbide by nanoindentation and Finite Element simulation, *Act. Materialia*, Vol. 58, pp. 3824-3832
- Shin, Y.C.; Pfefferkorn, F.E.; Rozzi, J.C. (2000). Experimental evaluation of laser assisted machining of Silicon Nitride ceramics, *Journal of Manufacturing Science- ASME*, Vol.122, pp. 666
- Sreejith, P.S.; Ngoi, B.K.A. (2001). Material removal mechanisms in precision machining of new materials, *International Journal of Machine Tools & Manufacture*, Vol.41, pp. 1831-1843
- Tsevetkov, V.F.; Allen, S.T.; Kong, H.S.; Carter, C.H. (1996). Recent progress in SiC crystal growth, *Institute of Physics*, Vol no. 142, pp.17
- Virkar, S.R.; Patten, J.A. (2009). Numerical simulations and analysis of thermal effects on Silicon Carbide during ductile mode micro-Laser Assisted Machining, *Proceedings of the ASME International Manufacturing Science and Engineering Conference*, West Lafayette, IN
- Virkar, S.R.; Patten, J.A. (2010). Simulation of thermal effects for analysis of micro Laser Assisted Machining, *Proceedings of ICOMM conference*, Madison, WI

- Wobker, H.G. & Tonshoff, H.K. (1993). High efficiency grinding of structural ceramics, *International Conference on Machining of Advanced Materials, NIST Special Publication 847*, pp. 455-463, Gaithersburg, MD.
- Yan, J.W.; Syoji, K. & Kuriyagawa, T. (2002). Ductile regime turning at large tool feed, *J. Mater. Process Tech.*, Vol. 121, No.2-3, pp. 363-372
- Yan, J.W.; Maekawa, K. & Tamaki, J.(2004). Experimental study on the ultra-precision ductile machinability of single-crystal germanium", *JSME International Journal C-Mech Sy.*, Vol.47, No.1, pp. 29-36
- Yonenaga, I. (2001). Thermo-Mechanical stability of wide-bandgap semiconductors: High temperature hardness of SiC, AlN, GaN, ZnO and ZnSe, *Physica B.*, 308-310, pp. 1150-1152

IntechOpen

IntechOpen

IntechOpen



Properties and Applications of Silicon Carbide

Edited by Prof. Rosario Gerhardt

ISBN 978-953-307-201-2

Hard cover, 536 pages

Publisher InTech

Published online 04, April, 2011

Published in print edition April, 2011

In this book, we explore an eclectic mix of articles that highlight some new potential applications of SiC and different ways to achieve specific properties. Some articles describe well-established processing methods, while others highlight phase equilibria or machining methods. A resurgence of interest in the structural arena is evident, while new ways to utilize the interesting electromagnetic properties of SiC continue to increase.

How to reference

In order to correctly reference this scholarly work, feel free to copy and paste the following:

Deepak Ravindra, Saurabh Virkar and John Patten (2011). Ductile Mode Micro Laser Assisted Machining of Silicon Carbide, Properties and Applications of Silicon Carbide, Prof. Rosario Gerhardt (Ed.), ISBN: 978-953-307-201-2, InTech, Available from: <http://www.intechopen.com/books/properties-and-applications-of-silicon-carbide/ductile-mode-micro-laser-assisted-machining-of-silicon-carbide>

INTECH
open science | open minds

InTech Europe

University Campus STeP Ri
Slavka Krautzeka 83/A
51000 Rijeka, Croatia
Phone: +385 (51) 770 447
Fax: +385 (51) 686 166
www.intechopen.com

InTech China

Unit 405, Office Block, Hotel Equatorial Shanghai
No.65, Yan An Road (West), Shanghai, 200040, China
中国上海市延安西路65号上海国际贵都大饭店办公楼405单元
Phone: +86-21-62489820
Fax: +86-21-62489821

© 2011 The Author(s). Licensee IntechOpen. This chapter is distributed under the terms of the [Creative Commons Attribution-NonCommercial-ShareAlike-3.0 License](#), which permits use, distribution and reproduction for non-commercial purposes, provided the original is properly cited and derivative works building on this content are distributed under the same license.

IntechOpen

IntechOpen